Higgs-photon associated production at $e\bar{e}$ colliders

Ali Abbasabadi[1], David Bowser-Chao[2], Duane A. Dicus[3] and

Wayne W. Repko[2]

[1]*Department of Physical Sciences*

Ferris State University, Big Rapids, Michigan 49307

[2]*Department of Physics and Astronomy*

Michigan State University, East Lansing, Michigan 48824

[3]*Center for Particle Physics and Department of Physics*

University of Texas, Austin, Texas 78712

(February 1, 2008)

Abstract

We present complete analytical expressions for the amplitudes of the process $e\bar{e} \to H\gamma$. The calculation is performed using nonlinear gauges, which significantly simplifies both the actual analytical calculation and the check of its gauge invariance. After comparing our results with a previous numerical calculation, we extend the range of Higgs masses and center of mass energies to those appropriate to LEP 200 and a future linear collider.

13.85.Qk, 14.80.Er, 14.80.Gt

I. INTRODUCTION

The search for the Higgs-boson (H) at $e\bar{e}$ colliders usually focuses on the channel $e\bar{e} \to Z \to Z^*H$ at the Z pole [1]. Some years ago, Barroso, Pulido and Romão [2] pointed out that the channel $e\bar{e} \to H\gamma$ could be important in Higgs searches, if for no other reason than that the range of accessible m_H is larger. These authors presented numerical results for relatively low Higgs masses ($m_H \leq 60$ GeV) and a top quark mass m_t of 40 GeV. They concluded the signal was observable and also drew attention to some interesting theoretical aspects of calculation related to gauge invariance with respect to the photon field.

Given the prospect of LEP 200 in the near term, the discussion of a higher energy $e\bar{e}$ collider (NLC) and an indication that $m_t \sim 175$ GeV [3], it seemed appropriate to revisit this calculation with the intention of extending the range of m_H and the center of mass energy $\sqrt{s}$. Accordingly, we have computed the amplitudes for $e\bar{e} \to H\gamma$ using two nonlinear gauges [4,5] for the W's. Our motivation for choosing nonlinear gauges was the reduction in the number of diagrams due to the elimination of W-neutral gauge boson-charged Goldstone boson couplings. We discovered that these gauges have the additional advantage of greatly simplifying the photon field gauge structure of the various classes of diagrams.

In the next Section, the choice of gauge fixing terms is presented and we outline the strategy of our calculation. We then present numerical results for a range of m_H and $e\bar{e}$ center of mass energies. The complete analytical expressions for the amplitudes are given in the Appendix.

II. NONLINEAR GAUGE FIXING AND CALCULATIONAL APPROACH

In the Standard Model, the lowest order corrections to the amplitudes for $e\bar{e} \to H\gamma$ come from one-loop diagrams containing various combinations of fermions, gauge bosons, Goldstone bosons ($G^\pm, G^0$) and ghosts ($\theta^\pm, \bar{\theta}^\pm, \eta_\gamma, \eta_Z$). Since the Born diagrams for this process are proportional to the electron mass m_e, the one-loop corrections actually determine

the amplitude in the $m_e \to 0$ limit. For the purposes of this calculation we generally set $m_e = 0$, although, as discussed below, some care must be exercised when doing so in one of the diagrams.

The precise number of diagrams encountered when computing the one-loop corrections is influenced by the choice of the gauge for the $W^\pm$ and Z^0. It has been shown that a carefully chosen nonlinear gauge [4] can eliminate the mixed W-G-γ vertices, reduce the number of diagrams and simplify the Feynman rules. More recently, a related nonlinear gauge has been introduced which also eliminates the W-G-Z vertices [5] and thereby further reduces the number of diagrams.

In this paper, we utilize nonlinear R_ξ gauges specified by gauge fixing terms of the form

$$\mathcal{L}_{GF} = -\frac{1}{2\xi_A}(f_A)^2 - \frac{1}{2\xi_Z}(f_Z)^2 - \frac{1}{\xi_W}ff^\dagger \, , \tag{1}$$

where, for either choice of nonlinear gauge,

$$f_A = \partial_\mu A_\mu \, , \tag{2}$$

$$f_Z = \partial_\mu Z_\mu + \xi_Z m_Z G^0 \, . \tag{3}$$

For the nonlinear gauges, we choose

$$f = \partial_\mu W_\mu - igW_\mu^3 W_\mu + i\xi_W m_W G \, , \tag{4}$$

or

$$f = \partial_\mu W_\mu - ig'B_\mu W_\mu + i\xi_W m_W G \, , \tag{5}$$

with

$$W_\mu^3 = \cos\theta_W Z_\mu + \sin\theta_W A_\mu \, , \tag{6}$$

$$B_\mu = -\sin\theta_W Z_\mu + \cos\theta_W A_\mu \, , \tag{7}$$

and θ_W denoting the weak mixing angle. The gauge parameters ξ_A, ξ_Z and ξ_W are all chosen to be unity, which corresponds to nonlinear 't Hooft-Feynman gauges. We obtain the ghost couplings for a particular nonlinear gauge by examining the revelant gauge fixing terms.

The diagrams encountered in the calculation of the $e\bar{e} \rightarrow H\gamma$ amplitudes fall into three catagories (illustrated in Fig. 1): those with two poles at m_Z; those with a single Z^0 or γ pole; and triangle or box diagrams with gauge bosons and fermions in the loops. Apart from a reduction in the number of diagrams to be calculated, the use of nonlinear gauges has the additional feature that these catagories are *separately* gauge invariant with respect to the photon field. This is not the case in linear gauges, where the replacement of the photon polarization vector $\hat{\epsilon}_\mu(k)$ by the momentum vector k_μ mixes contributions from various catagories to produce the expected zero result.

It is worth mentioning that the separation of the diagrams into gauge invariant subsets can be traced to the simplified Ward identity satisfied by the W-W-γ vertex in either nonlinear gauge. Specifically, if $\Gamma_{\mu\nu\lambda}(p+k,p)$ denotes the vertex function for an incoming W with momentum p and polarization $\hat{\epsilon}_\nu(p)$, an outgoing W of momentum $p+k$ and polarization $\hat{\epsilon}_\mu(p+k)$ and a photon of momentum k and polarization $\hat{\epsilon}_\lambda(k)$, the Ward identity is

$$k_\lambda \Gamma_{\mu\nu\lambda}(p+k,p) = e\delta_{\mu\nu}[\Delta_F^{-1}(p+k) - \Delta_F^{-1}(p)] , \tag{8}$$

where

$$\Delta_F^{-1}(p) = p^2 + m_W^2 . \tag{9}$$

The simplicity of the righthand side of Eq.(8) means that the replacement of the photon polarization vector $\hat{\epsilon}(k)$ by the momentum k merely eliminates one or the other of the propagators adjacent to the vertex. There are no extra contributions which serve to connect one catagory of diagrams to another.

A. Double pole diagrams

One consequence of the separation mentioned above is that the double pole diagrams illustrated in Fig. 1(a) vanish when the photon is on the mass shell. There is no need to perform a renormalization, unlike the situation found in Ref. [2].

On the photon mass shell, any given double pole diagram makes a contribution of the general form

$$\mathcal{M}_{\mu\nu} = (eg^2/m_Z)(\alpha + \beta\tan^2\theta_W)\delta_{\mu\nu}. \tag{10}$$

The coefficients α and β are expressible in terms of the scalar loop integrals $A_0(m_W^2) = A_0$ and $B_0(k^2 = 0, m_W^2, m_W^2) = B_0$ of 't Hooft and Veltman [6]. Although A_0 and B_0 depend on the number of dimensions n, they satisfy the relation

$$(1 - \frac{n}{2})A_0 - m_W^2 B_0 = 0 . \tag{11}$$

The contributions of the non-vanishing diagrams are listed in Table I. These consist of tadpole and bubble diagrams with W's, charged Goldstone bosons or ghosts in the loops. Notice that for each particle the sum of the one-point and two-point contributions results in the combination Eq. (11). Consequently, the double pole diagrams all vanish.

B. Single pole diagrams

The single pole diagrams of Fig. 1(b) involve Z^0 or γ poles, with the virtual gauge boson of momentum p decaying into $H\gamma$ (momenta k' and k). Our result for the $\gamma^* \to H\gamma$ amplitude is gauge invariant, in agreement with Ref. [2]. Unlike Ref. [2], we also find the $Z^* \to H\gamma$ amplitude to be gauge invariant. In the nonlinear gauges there is no need to combine this contribution with box contributions to achieve a gauge invariant result.

The relevant diagrams consist of quark, W, Goldstone boson and ghost loops, which we evaluate using the Passarino and Veltman decomposition [7]. The complete contribution from the photon pole is

$$\begin{aligned}
\mathcal{M}_{\text{Pole}}^{\gamma} = {}& \frac{\alpha^2 m_W}{\sin\theta_W}\bar{v}(p_2)\gamma_\mu u(p_1)\hat{\epsilon}_\nu(k)\Big(\frac{\delta_{\mu\nu}k\cdot(p_1+p_2) - k_\mu(p_1+p_2)_\nu}{s}\Big) \\
& \times \Big\{4(6 + \frac{m_H^2}{m_W^2})C_{23}(s, m_H^2, m_W^2) - 16C_0(s, m_H^2, m_W^2) \\
& - \frac{8}{3}\frac{m_t^2}{m_W^2}\Big(4C_{23}(s, m_H^2, m_t^2) - C_0(s, m_H^2, m_t^2)\Big)\Big\} ,
\end{aligned} \tag{12}$$

where $s = -(p_1 + p_2)^2$ and $C_0(s, m_H^2, m^2)$ and $C_{23}(s, m_H^2, m^2)$ are scalar functions given in the Appendix A.

For the Z^0 pole contribution, we find

$$
\begin{aligned}
\mathcal{M}^Z_{\text{Pole}} = {} & \frac{\alpha^2 m_W}{\sin^3 \theta_W} \bar{v}(p_2) \gamma_\mu (v_e + \gamma_5) u(p_1) \hat{\epsilon}_\nu(k) \left(\frac{\delta_{\mu\nu} k \cdot (p_1 + p_2) - k_\mu (p_1 + p_2)_\nu}{s - m_Z^2 + i m_Z \Gamma_Z} \right) \\
& \times \left\{ \left((6 - \frac{1}{\cos^2 \theta_W}) + \frac{m_H^2}{2 m_W^2} \frac{1 - 2 \sin^2 \theta_W}{\cos^2 \theta_W} \right) C_{23}(s, m_H^2, m_W^2) \right. \\
& + \left(\frac{1}{\cos^2 \theta_W} - 4 \right) C_0(s, m_H^2, m_W^2) \\
& \left. - \frac{1}{4} \frac{m_t^2}{m_W^2} \frac{1 - (8/3) \sin^2 \theta_W}{\cos^2 \theta_W} \left(4 C_{23}(s, m_H^2, m_t^2) - C_0(s, m_H^2, m_t^2) \right) \right\} .
\end{aligned}
\tag{13}
$$

Here, $v_e = 1 - 4 \sin^2 \theta_W$ and Γ_Z denotes the Z^0 width.

C. Box and associated triangle diagrams

The remaining diagrams (Fig. 1 (c)) have no gauge boson poles. They consist of box diagrams where the photon emerges from one of the box vertices together with associated triangle diagrams with the photon being radiated by one of the incoming leptons. There are two such combinations of boxes and triangles: one with Z's in the loops and one with W's in the loops.

The contribution to the matrix element from the box and triangles with internal Z's is given by

$$
\begin{aligned}
\mathcal{M}^Z_{\text{Box}} = {} & -\frac{\alpha^2 m_Z}{4 \sin^3 \theta_W \cos^3 \theta_W} \bar{v}(p_2) \gamma_\mu (v_e + \gamma_5)^2 u(p_1) \hat{\epsilon}_\nu(k) \\
& \times \left\{ \left(\delta_{\mu\nu} k \cdot p_1 - k_\mu (p_1)_\nu \right) A(s, t, u) + \left(\delta_{\mu\nu} k \cdot p_2 - k_\mu (p_2)_\nu \right) A(s, u, t) \right\} ,
\end{aligned}
\tag{14}
$$

with $t = -(p_1 - k)^2$ and $u = -(p_2 - k)^2$. The scalar function $A(s, t, u)$ is given in the Appendix B. In the evaluation of the loop integrals for this contribution, we encountered $\ln(m_e^2)$ terms in the box diagram. These were shown to cancel in the final result and we then set $m_e = 0$ in the remaining expressions. Notice, too, that Eq. (14) is explicitly gauge invariant.

6

The contribution from the diagrams with internal W's is also gauge invariant and given by

$$
\begin{aligned}
\mathcal{M}^W_{\text{Box}} = \ & \frac{\alpha^2 m_W}{2 \sin^3 \theta_W} \bar{v}(p_2) \gamma_\mu (1 + \gamma_5)^2 u(p_1) \hat{\epsilon}_\nu(k) \\
& \times \left\{ \left(\delta_{\mu\nu} k \cdot p_1 - k_\mu (p_1)_\nu \right) \left(A_1(s,t,u) + A_2(s,u,t) \right) \right. \\
& \left. + \left(\delta_{\mu\nu} k \cdot p_2 - k_\mu (p_2)_\nu \right) \left(A_2(s,t,u) + A_1(s,u,t) \right) \right\} ,
\end{aligned}
\tag{15}
$$

with expressions for $A_1(s,t,u)$ and $A_2(s,t,u)$ given in the Appendix C.

All expressions for the scalar functions given in the Appendices have been checked numerically using Veltman's program FORMF [8] and Vermaseren's program FF [9]. The results presented below were obtained using the formulae in Appendices A-C.

III. DISCUSSION

The differential cross section $d\sigma(e\bar{e} \to H\gamma)/d\Omega_\gamma$ is given by

$$
\frac{d\sigma(e\bar{e} \to H\gamma)}{d\Omega_\gamma} = \frac{1}{256\pi^2} \frac{s - m_H^2}{s^2} \sum_{\text{spin}} |\mathcal{M}|^2 ,
\tag{16}
$$

where the invariant amplitude $\mathcal{M}$ is the sum of Eqs. (12-15). Explicitly, we have

$$
\begin{aligned}
\sum_{\text{spin}} |\mathcal{M}|^2 = \ & \frac{\alpha^4 m_W^2 s}{16 \sin^6 \theta_W \cos^8 \theta_W} \left\{ (t^2 + u^2) \left(|\mathcal{A}_\gamma|^2 + 2 v_e \text{Re}(\mathcal{A}_\gamma \mathcal{A}_Z^*) + (1 + v_e^2) |\mathcal{A}_Z|^2 \right) \right. \\
& + t^2 \left[2(1 + v_e^2) \text{Re}(\mathcal{A}_\gamma \mathcal{A}^*) + 4 \text{Re}(\mathcal{A}_\gamma \mathcal{A}_{12}^*) + 2(v_e^3 + 3 v_e) \text{Re}(\mathcal{A}_Z \mathcal{A}^*) \right. \\
& + 4(1 + v_e) \text{Re}(\mathcal{A}_Z \mathcal{A}_{12}^*) + (1 + 6 v_e^2 + v_e^4) |\mathcal{A}|^2 + 4(1 + v_e)^2 \text{Re}(\mathcal{A} \mathcal{A}_{12}^*) \\
& \left. \left. + 8 |\mathcal{A}_{12}|^2 \right] + u^2 \left[t \leftrightarrow u \right] \right\} .
\end{aligned}
\tag{17}
$$

Here, $\mathcal{A}_\gamma$, $\mathcal{A}_Z$, $\mathcal{A}$ and $\mathcal{A}_{12}$ are

$$
\mathcal{A}_\gamma = 4 \sin^2 \theta_W \cos^4 \theta_W \frac{1}{s} \times \{ \cdots \} ,
\tag{18}
$$

$$
\mathcal{A}_Z = 4 \cos^4 \theta_W \frac{1}{s - m_Z^2 + i m_Z \Gamma_Z} \times \{ \cdots \} ,
\tag{19}
$$

$$
\mathcal{A} = A(s,t,u) , \quad (\text{Eq.(B2)}) ,
\tag{20}
$$

$$
\mathcal{A}_{12} = -2 \cos^4 \theta_W \left(A_1(s,t,u) + A_2(s,u,t) \right) \quad (\text{Eqs.(C3) \& (C4)}) ,
\tag{21}
$$

7

and $\{\cdots\}$ in Eqs. (18) and (19) denotes the contents of the curly brackets in Eqs. (12) and (13), respectively.

For purposes of comparison with Table 4 of Ref. [2], Eq. (16) was used to compute $\sigma(e\bar{e} \to H\gamma)$ when $m_H = m_t = 40$ GeV and 60 GeV $\leq \sqrt{s} \leq 150$ GeV. The two sets of results are given in Table II. From this data, it is evident that there are differences between the two calculations on a contribution-by-contribution basis. We attribute this variation to the fact that the $\mathcal{M}^Z_{\text{Pole}}$ and $\mathcal{M}^Z_{\text{Box}}$ are not separately gauge invariant for the linear 't Hooft-Feynman gauge of Ref. [2]. These amplitudes are separately gauge invariant for the nonlinear 't Hooft-Feynman gauges used in the present calculation. The total cross section for the two cases is plotted in Fig. 2. The results are in good agreement, although the cross section of Ref. [2] is slightly lower than ours both below and above the Z peak.

In Fig. 3, the cross sections corresponding to $m_H = 60, 80, 100, 120$ and 150 GeV are plotted for the LEP 200 range $\sqrt{s} \leq 200$ GeV using a top quark mass of 174 GeV. Apart from $m_H = 150$ GeV, the cross sections rise to a level greater than 0.1 fb as $\sqrt{s} \to 200$ GeV. The only discernible feature above the Z peak is the $2W$ threshold at $\sqrt{s} \sim 160$ GeV.

The extension to the range $\sqrt{s} \leq 500$ GeV is shown in Fig. 4. All curves clearly show the effect of the top threshold. In addition, the $m_H = 2M_Z$ curve forms a new upper envelope for the cross sections corresponding to the region $m_H \geq 2m_Z$.

The cross sections are, of course, quite small. At expected LEP 200 luminosities (0.5 - 1.0 fb^{-1}) no events of this type should be seen. Thus, any observed $H\gamma$ events would be a signal of new physics. For proposed NLC luminosities (50 fb^{-1}/yr), $H\gamma$ events should be seen. At other energies or masses, our analytic results allow the cross section to be determined easily.

APPENDIX A: SINGLE POLE DIAGRAM INTEGRALS

When evaluating the gauge boson pole contributions, we encounter the functions $C_0(s, m_H^2, m^2)$ and $C_{23}(s, m_H^2, m^2)$. These functions are defined in terms of loop integrals as

$$C_0(s, m_H^2, m^2) = \frac{1}{i\pi^2} \int d^n q \frac{1}{(q^2 + m^2)((q-p)^2 + m^2)((q-k)^2 + m^2)} , \tag{A1}$$

$$C_{\mu\nu}(p, k) = \frac{1}{i\pi^2} \int d^n q \frac{q_\mu q_\nu}{(q^2 + m^2)((q-p)^2 + m^2)((q-k)^2 + m^2)} \tag{A2}$$

$$= C_{21}(s, m_H^2, m^2) p_\mu p_\nu + C_{22}(s, m_H^2, m^2) k_\mu k_\nu +$$

$$C_{23}(s, m_H^2, m^2)(p_\mu k_\nu + k_\mu p_\nu) + C_{24}(s, m_H^2, m^2)\delta_{\mu\nu} ,$$

where we have used $p^2 = -s$ and the mass shell conditions $k'^2 = -m_H^2$, $k^2 = 0$. The latter enables us to eliminate reference to the k^2 dependence of the C's. It should be noted that numerous other C's appear in the course of the calculation, but only C_0 and C_{23} survive in the final result.

The evaluation of $C_0(s, m_H^2, m^2)$ is straightforward, yielding

$$C_0(s, m_H^2, m^2) = \frac{1}{(s - m_H^2)}\Big(C(\frac{m_H^2}{m^2}) - C(\frac{s}{m^2})\Big) , \tag{A3}$$

where

$$C(\beta) = \int_0^1 \frac{dx}{x} \ln\Big(1 - \beta x(1-x) - i\varepsilon\Big) \tag{A4}$$

$$= \begin{cases} -2\Big(\sin^{-1}(\sqrt{\frac{\beta}{4}})\Big)^2 & 0 \le \beta \le 4 \\ 2\Big(\cosh^{-1}(\sqrt{\frac{\beta}{4}})\Big)^2 - \frac{\pi^2}{2} - 2i\pi \cosh^{-1}(\sqrt{\frac{\beta}{4}}) & \beta \ge 4 \end{cases} . \tag{A5}$$

By analyzing Eq.(A2), it can be shown that $C_{23}(s, m_H^2, m^2)$ is expressible as

$$C_{23}(s, m_H^2, m^2) = -\frac{1}{2(s - m_H^2)}\left[-(2 - \frac{n}{2})B_0(k'^2, m^2) + 2m^2 C_0(s, m_H^2, m^2)\right. \tag{A6}$$

$$\left.+\frac{s}{(s - m_H^2)}\left(B_0(k'^2, m^2) - B_0(p^2, m^2)\right)\right] .$$

The two-point scalar function $B_0(p^2, m^2)$ is defined by

$$B_0(p^2, m^2) = \frac{1}{i\pi^2}\int d^n q \frac{1}{(q^2 + m^2)((q + p)^2 + m^2)} . \tag{A7}$$

This integral can be evaluated to give

$$B_0(p^2, m^2) = \frac{\pi^{(n/2-2)}\Gamma(2 - \frac{n}{2})}{(m^2)^{(2-n/2)}} - B(-\frac{p^2}{m^2}) , \tag{A8}$$

with

$$B(\beta) = \int_0^1 dx \ln(1 - \beta x(1 - x) - i\varepsilon) \tag{A9}$$

$$= \begin{cases} 2\left[\sqrt{\frac{4-\beta}{\beta}}\sin^{-1}(\sqrt{\frac{\beta}{4}}) - 1\right] & 0 \le \beta \le 4 \\ 2\left[\sqrt{\frac{\beta-4}{\beta}}\cosh^{-1}(\sqrt{\frac{\beta}{4}}) - 1 - \frac{i\pi}{2}\sqrt{\frac{\beta-4}{\beta}}\right] & \beta \ge 4 \end{cases} . \tag{A10}$$

$C_{23}(s, m_H^2, m^2)$ then takes the form

$$C_{23}(s, m_H^2, m^2) = \frac{1}{2}\frac{1}{(s - m_H^2)}\left[1 + \frac{s}{(s - m_H^2)}\left(B(\frac{m_H^2}{m^2}) - B(\frac{s}{m^2})\right)\right. \tag{A11}$$

$$\left.-\frac{2m^2}{(s - m_H^2)}\left(C(\frac{m_H^2}{m^2}) - C(\frac{s}{m^2})\right)\right] .$$

APPENDIX B: Z BOX

The diagrams with Z's in the loop consist of the crossed box illustrated in the first of Figs. 1 (c) and two triangle diagrams of the type shown in the last of Figs. 1 (c). In the nonlinear gauges, the triangle contributions serve to cancel a non-gauge-invariant term in the crossed box. The entire contribution is given by the function $A(s, t, u)$, which appears in Eq. (14). In terms of the decomposition of Ref. [7], this function is given by

$$A(s, t, u) = D_0(s, t, u, m_H^2, m_e^2, m_Z^2) + D_{11}(s, t, u, m_H^2, m_e^2, m_Z^2) \tag{B1}$$

$$+D_{12}(s, t, u, m_H^2, m_e^2, m_Z^2) + D_{24}(s, t, u, m_H^2, m_e^2, m_Z^2) .$$

10

When the $D_{\alpha\beta}$ in Eq. (B1) are expanded in terms of scalar integrals, the expression for $A(s,t,u)$ takes the form

$$A(s,t,u) = \frac{1}{2}\frac{1}{st}\left[\frac{1}{t}(t-m_Z^2)\left(m_Z^2(t+u)-tu\right)D_0(1,2,3,4) - (t-m_Z^2)C_0(1,2,3)\right.$$
$$-\frac{1}{t}\left((t-m_Z^2)(s-t)-2m_Z^2\frac{st}{(s+t)}\right)C_0(1,2,4)+\frac{1}{t}(t-m_Z^2)(s+u)C_0(1,3,4)$$
$$\left.-\frac{u}{t}(t-m_Z^2)C_0(2,3,4)+\frac{2s}{(s+t)}\left(B_0(1,4)-B_0(2,4)\right)\right], \tag{B2}$$

where we have used the compact notation of Ref. [7] with $m_1 = m_4 = m_Z$ and $m_2 = m_3 = m_e$. This labeling is illustrated in Fig. 5 (a).

Explicit evaluation of $D_0(1,2,3,4)$ gives

$$D_0(1,2,3,4) = \frac{1}{(tu-m_Z^2 t-m_Z^2 u)}\left\{\left[\ln\left(1-\frac{t}{m_Z^2}\right)\left(\ln\left(\frac{tu}{m_e^2 m_H^2}\right)+2\ln\left(1-\frac{m_Z^2}{t}\right)\right.\right.\right.$$
$$+\ln\left(-\frac{m_Z^2}{t}\right)+\ln\left(1-\frac{m_Z^2}{t}-\frac{m_Z^2}{u}\right)-\ln\left(\beta_+-\frac{m_Z^2}{t}\right)-\ln\left(\beta_--\frac{m_Z^2}{t}\right)\right)$$
$$+2Li_2\left(\frac{-\frac{m_Z^2}{t}}{1-\frac{m_Z^2}{t}}\right)+Li_2\left(\frac{-\frac{m_Z^2}{t}}{1-\frac{m_Z^2}{t}-\frac{m_Z^2}{u}}\right)-Li_2\left(\frac{-\frac{m_Z^2}{t}}{\beta_+-\frac{m_Z^2}{t}}\right)$$
$$-Li_2\left(\frac{-\frac{m_Z^2}{t}}{\beta_--\frac{m_Z^2}{t}}\right)-Li_2\left(\frac{1-\frac{m_Z^2}{t}}{1-\frac{m_Z^2}{t}-\frac{m_Z^2}{u}}\right)$$
$$+Li_2\left(\frac{1-\frac{m_Z^2}{t}}{\beta_+-\frac{m_Z^2}{t}+i\varepsilon}\right)+Li_2\left(\frac{1-\frac{m_Z^2}{t}}{\beta_--\frac{m_Z^2}{t}-i\varepsilon}\right)-\frac{\pi^2}{3}\right]+[t\leftrightarrow u]\right\}, \tag{B3}$$

where $Li_2(z)$ is the dilogarithm or Spence function [10] defined by

$$Li_2(z) = -\int_0^1 \frac{dt}{t}\ln(1-zt). \tag{B4}$$

Notice that $D_0(1,2,3,4)$ has a $\ln(m_e^2)$ dependence, which eventually cancels as shown below. The roots $\beta_\pm$ are

$$\beta_\pm = \frac{1}{2}\left(1\pm\sqrt{1-\frac{4m_Z^2}{m_H^2}}\right). \tag{B5}$$

The various C_0 functions are

11

$$C_0(1,2,3) = \frac{1}{t}\left[Li_2\left(\frac{1}{1-\frac{m_Z^2}{t}}\right) - \frac{1}{2}\ln^2\left(1-\frac{t}{m_Z^2}\right) + \ln\left(1-\frac{t}{m_Z^2}\right)\ln\left(\frac{m_e^2}{m_Z^2}\right)\right], \qquad \text{(B6)}$$

$$\begin{aligned}
C_0(1,2,4) = \ \frac{1}{m_H^2-u}&\left[-Li_2\left(\frac{\alpha_1-1}{\alpha_1-i\varepsilon}\right) - Li_2\left(\frac{\alpha_2}{\alpha_2-\beta_-+i\varepsilon}\right)\right.\\
&+Li_2\left(\frac{\alpha_2-1}{\alpha_2-\beta_-+i\varepsilon}\right) - Li_2\left(\frac{\alpha_2}{\alpha_2-\beta_+-i\varepsilon}\right)\\
&+Li_2\left(\frac{\alpha_2-1}{\alpha_2-\beta_+-i\varepsilon}\right) + Li_2\left(\frac{\alpha_3}{\alpha_3-1+i\varepsilon}\right)\\
&\left.+Li_2\left(\frac{\alpha_3}{\alpha_3-\frac{m_Z^2}{u}-i\varepsilon}\right) - Li_2\left(\frac{\alpha_3-1}{\alpha_3-\frac{m_Z^2}{u}-i\varepsilon}\right)\right],
\end{aligned} \qquad \text{(B7)}$$

$$\begin{aligned}
C_0(1,3,4) = \ \frac{1}{m_H^2-t}&\left[-Li_2\left(\frac{\gamma-1}{\gamma-1+\frac{m_Z^2}{t}+i\varepsilon}\right) + Li_2\left(\frac{\gamma}{\gamma-1+\frac{m_Z^2}{t}+i\varepsilon}\right)\right.\\
&-Li_2\left(\frac{\gamma-1}{\gamma-i\varepsilon}\right) - Li_2\left(\frac{\gamma}{\gamma-\beta_-+i\varepsilon}\right)\\
&+Li_2\left(\frac{\gamma-1}{\gamma-\beta_-+i\varepsilon}\right) - Li_2\left(\frac{\gamma}{\gamma-\beta_+-i\varepsilon}\right)\\
&\left.+Li_2\left(\frac{\gamma-1}{\gamma-\beta_+-i\varepsilon}\right) + \frac{\pi^2}{6}\right],
\end{aligned} \qquad \text{(B8)}$$

$$C_0(2,3,4) = \frac{1}{u}\left[Li_2\left(\frac{1}{1-\frac{m_Z^2}{u}}\right) - \frac{1}{2}\ln^2\left(1-\frac{u}{m_Z^2}\right) + \ln\left(1-\frac{u}{m_Z^2}\right)\ln\left(\frac{m_e^2}{m_Z^2}\right)\right]. \qquad \text{(B9)}$$

The roots α_1, α_2, α_3 and γ are

$$\begin{aligned}
\alpha_1 &= \frac{u^2 - m_H^2 u + m_Z^2 m_H^2}{(m_H^2-u)^2}, & \alpha_2 &= \frac{m_Z^2}{(m_H^2-u)},\\
\alpha_3 &= \frac{m_Z^2 m_H^2}{u(m_H^2-u)}, & \gamma &= \frac{m_Z^2}{(m_H^2-t)},
\end{aligned} \qquad \text{(B10)}$$

and the roots $\beta_\pm$ are those of Eq. (B5). Note that $C_0(1,2,4)$ can also be obtained directly from $C_0(1,3,4)$ by replacing t with u.

Finally, the required B_0 functions are

$$B_0(1,4) = \Delta + \beta_+ \ln\left(\frac{\beta_+ - 1 + i\varepsilon}{\beta_+}\right) + \beta_- \ln\left(\frac{\beta_- - 1 - i\varepsilon}{\beta_-}\right) + 2, \tag{B11}$$

$$B_0(2,4) = \Delta + \left(1 - \frac{m_Z^2}{u}\right) \ln\left(\frac{m_Z^2}{m_Z^2 - u}\right) + 2, \tag{B12}$$

where Δ is

$$\Delta = \pi^{(n/2-2)}\Gamma\left(2 - \frac{n}{2}\right), \tag{B13}$$

and, again, $\beta_\pm$ are given in Eq. (B5).

The cancellation of the $\ln(m_e^2)$ dependence of Eqs. (B3), (B6) and (B9) can be checked by substituting the explicit expressions into Eq. (B2).

APPENDIX C: W BOX

The diagrams with W's in the loop are the box diagram shown in the second of Figs. 1 (c) and the triangle diagram given in the last of Figs. 1 (c), together with their counterparts having the Higgs and photon interchanged. The non-gauge-invariant part of each box diagram is canceled by the corresponding triangle diagram. The W contribution is determined by two scalar functions $A_1(s,t,u)$ and $A_2(s,t,u)$, which appear in Eq. (15). These functions can be related to the $D_{\alpha\beta}$ of Ref. [7] as

$$A_1(s,t,u) = D_0(s,t,u,m_H^2,m_e^2,m_W^2) + D_{11}(s,t,u,m_H^2,m_e^2,m_W^2)$$
$$+D_{13}(s,t,u,m_H^2,m_e^2,m_W^2) + D_{25}(s,t,u,m_H^2,m_e^2,m_W^2), \tag{C1}$$

$$A_2(s,t,u) = -D_{12}(s,t,u,m_H^2,m_e^2,m_W^2) + D_{13}(s,t,u,m_H^2,m_e^2,m_W^2)$$
$$+D_{26}(s,t,u,m_H^2,m_e^2,m_W^2). \tag{C2}$$

The decomposition into scalar functions takes the form

$$A_1(s,t,u) = \frac{1}{2}\frac{1}{st}\left[\left(\frac{(s+t-m_W^2)}{t}\left(m_W^2(t+u) - su\right) - 2m_W^2 s\right)D_0(1,2,3,4)\right.$$
$$\left. +(s+t-m_W^2)\left[-\frac{s}{t}C_0(1,2,3) + \frac{(s^2 + 2st - t^2)}{(s+t)t}C_0(1,2,4)\right.\right. \tag{C3}$$

13

$$+\frac{(t+u)}{t}C_0(1,3,4)-\frac{u}{t}C_0(2,3,4)\Big]$$

$$+\frac{2s}{(t+u)}\left(B_0(1,3)-B_0(1,4)\right)+\frac{2s}{(s+t)}\left(B_0(2,4)-B_0(1,4)\right)\Big],$$

$$A_2(s,t,u)=\ \frac{1}{2}\frac{1}{su}\Big[\frac{(u-m_W^2)}{u}\left(su+m_W^2(t+u)\right)D_0(1,2,3,4)$$

$$+(u-m_W^2)\Big[\frac{s}{u}C_0(1,2,3)-\frac{(s+t)}{u}C_0(1,2,4) \tag{C4}$$

$$+\frac{(t+u)}{u}C_0(1,3,4)-C_0(2,3,4)\Big]$$

$$+\frac{2s}{(t+u)}\left(B_0(1,4)-B_0(1,3)\right)\Big].$$

In this case, $m_1=m_3=m_4=m_W$ and $m_2=m_\nu=0$ and we follow the labeling in Fig. 5 (b).

The expression for $D_0(1,2,3,4)$ is

$$D_0(1,2,3,4)=\ -\frac{1}{su(\lambda_+-\lambda_-)}\bigg\{\Big[-Li_2\left(\frac{1-\lambda_+}{\alpha-\lambda_+-i\varepsilon}\right)+Li_2\left(\frac{-\lambda_+}{\alpha-\lambda_+-i\varepsilon}\right)$$

$$-Li_2\left(\frac{1-\lambda_+}{\gamma_+-\lambda_++i\varepsilon}\right)+Li_2\left(\frac{-\lambda_+}{\gamma_+-\lambda_++i\varepsilon}\right)$$

$$-Li_2\left(\frac{1-\lambda_+}{\gamma_--\lambda_+-i\varepsilon}\right)+Li_2\left(\frac{-\lambda_+}{\gamma_--\lambda_+-i\varepsilon}\right) \tag{C5}$$

$$+Li_2\left(\frac{1-\lambda_+}{\beta_+-\lambda_++i\varepsilon}\right)-Li_2\left(\frac{-\lambda_+}{\beta_+-\lambda_++i\varepsilon}\right)$$

$$+Li_2\left(\frac{1-\lambda_+}{\beta_--\lambda_+-i\varepsilon}\right)-Li_2\left(\frac{-\lambda_+}{\beta_--\lambda_+-i\varepsilon}\right)\Big]$$

$$-\Big[\lambda_+\to\lambda_-\Big]\bigg\},$$

and the roots α, $\beta_\pm$, $\gamma_\pm$ and $\lambda_\pm$ are

$$\alpha=\ 1-\frac{m_W^2}{u}, \tag{C6}$$

$$\beta_\pm=\ \frac{1}{2}\left(1\pm\sqrt{1-\frac{4m_W^2}{m_H^2}}\right), \tag{C7}$$

$$\gamma_\pm=\ \frac{1}{2}\left(1\pm\sqrt{1-\frac{4m_W^2}{s}}\right), \tag{C8}$$

$$\lambda_\pm=\ \frac{1}{2}\left(1+\frac{m_W^2(s-m_H^2)}{-su}\pm\sqrt{\left(1+\frac{m_W^2(s-m_H^2)}{-su}\right)^2-\frac{4m_W^2}{s}}\right). \tag{C9}$$

14

The C_0's in this case are

$$
\begin{aligned}
C_0(1,2,3) = \ & \frac{1}{s}\left[\frac{\pi^2}{6} - Li_2\left(1 - \frac{s}{m_W^2}\right) - Li_2\left(\frac{m_W^2}{m_W^2 - s\gamma_+ - i\varepsilon}\right)\right. \\
& + Li_2\left(\frac{m_W^2 - s}{m_W^2 - s\gamma_+ - i\varepsilon}\right) - Li_2\left(\frac{m_W^2}{m_W^2 - s\gamma_- + i\varepsilon}\right) \\
& \left. + Li_2\left(\frac{m_W^2 - s}{m_W^2 - s\gamma_- + i\varepsilon}\right)\right],
\end{aligned}
\tag{C10}
$$

$$
\begin{aligned}
C_0(1,3,4) = \ & \frac{1}{m_H^2 - s}\left[-Li_2\left(\frac{1}{\gamma_+ + i\varepsilon}\right) - Li_2\left(\frac{1}{\gamma_- - i\varepsilon}\right)\right. \\
& \left. + Li_2\left(\frac{1}{\beta_+ + i\varepsilon}\right) + Li_2\left(\frac{1}{\beta_- - i\varepsilon}\right)\right],
\end{aligned}
\tag{C11}
$$

$$
C_0(2,3,4) = \frac{1}{u}Li_2\left(\frac{u}{m_W^2}\right),
\tag{C12}
$$

and $C_0(1,2,4)$ being given by Eq. (B7) with $m_Z \to m_W$.

Lastly, the B_0's are

$$
B_0(1,3) = \Delta + \gamma_+ \ln\left(\frac{\gamma_+ - 1 + i\varepsilon}{\gamma_+}\right) + \gamma_- \ln\left(\frac{\gamma_- - 1 - i\varepsilon}{\gamma_-}\right) + 2,
\tag{C13}
$$

$$
B_0(1,4) = \Delta + \beta_+ \ln\left(\frac{\beta_+ - 1 + i\varepsilon}{\beta_+}\right) + \beta_- \ln\left(\frac{\beta_- - 1 - i\varepsilon}{\beta_-}\right) + 2,
\tag{C14}
$$

$$
B_0(2,4) = \Delta + \left(1 - \frac{m_W^2}{u}\right) \ln\left(\frac{m_W^2}{m_W^2 - u}\right) + 2,
\tag{C15}
$$

where $\beta_\pm$ is given by Eq. (C7) and Δ by Eq. (B13).

15

REFERENCES

[1] G. Giacomelli and P. Giacomelli, CERN preprint CERN-PPE/93-107 (1993).

[2] A. Barroso, J. Pulido and J. C. Romão, Nucl. Phys. **B267**, 509 (1986).

[3] F. Abe *et al.* (CDF Collaboration), Phys. Rev. Lett. **73**, 225 (1994).

[4] K. Fujikawa, Phys. Rev. D **7**, 393 (1973); M. Bace and N. D. Hari Dass, Ann. of Phys. **94**, 349 (1975); M. B. Gavela, G. Girardi, C. Malleville, and P. Sorba, Nucl. Phys. **B193**, 257 (1981); N. G. Deshpande and M. Nazerimonfared, Nucl. Phys. **B213**, 390 (1983).

[5] D. A. Dicus and C. Kao, Phys. Rev. D **49**, 1265 (1994).

[6] G. 't Hooft and M. Veltman, Nucl. Phys. **B153**, 365 (1979).

[7] G. Passarino and M. Veltman, Nucl. Phys. **B160**, 151 (1979).

[8] D. A. Dicus and C. Kao, LOOP, a FORTRAN program for doing loop integrations of 1, 2, 3, and 4 point functions with momenta in the numerator, 1991 (unpublished).

[9] G. J. van Oldenborgh and J.A.M. Vermaseren, Zeit. Phys. C **46**, 425 (1990).

[10] R. Lewin, *Polylogarithms and Associated Functions* North Holland, New York, N. Y. (1981).

FIGURES

FIG. 1. Typical diagrams for the double pole (a), single pole (c) and box (c) corrections are shown. An external soild line represents an electron, a wavy line a gauge boson, a dashed line a Higgs boson and an internal solid line a fermion, gauge boson, Goldsone boson or ghost.

FIG. 2. The cross section from the present calculation (solid line) is compared with the result from Ref. [2] (dashed line).

FIG. 3. $\sigma(e\bar{e} \rightarrow \gamma H)$ is plotted for $m_H = 60$ (solid), 80 (dashed), 100 (long dashed), 120 (dot dashed), and 150 (dot dot dashed) GeV.

FIG. 4. $\sigma(e\bar{e} \rightarrow \gamma H)$ is plotted for $m_H = 60$ (solid), 80 (dashed), 100 (long dashed), 120 (dot dashed), 150 (dot dot dashed), $2m_Z$ (dotted), and 250 (short dashed) GeV.

FIG. 5. The numbering scheme used for the computation of $D_0(1, 2, 3, 4)$ in the case of the Z box (a) and the W box (b) are shown.
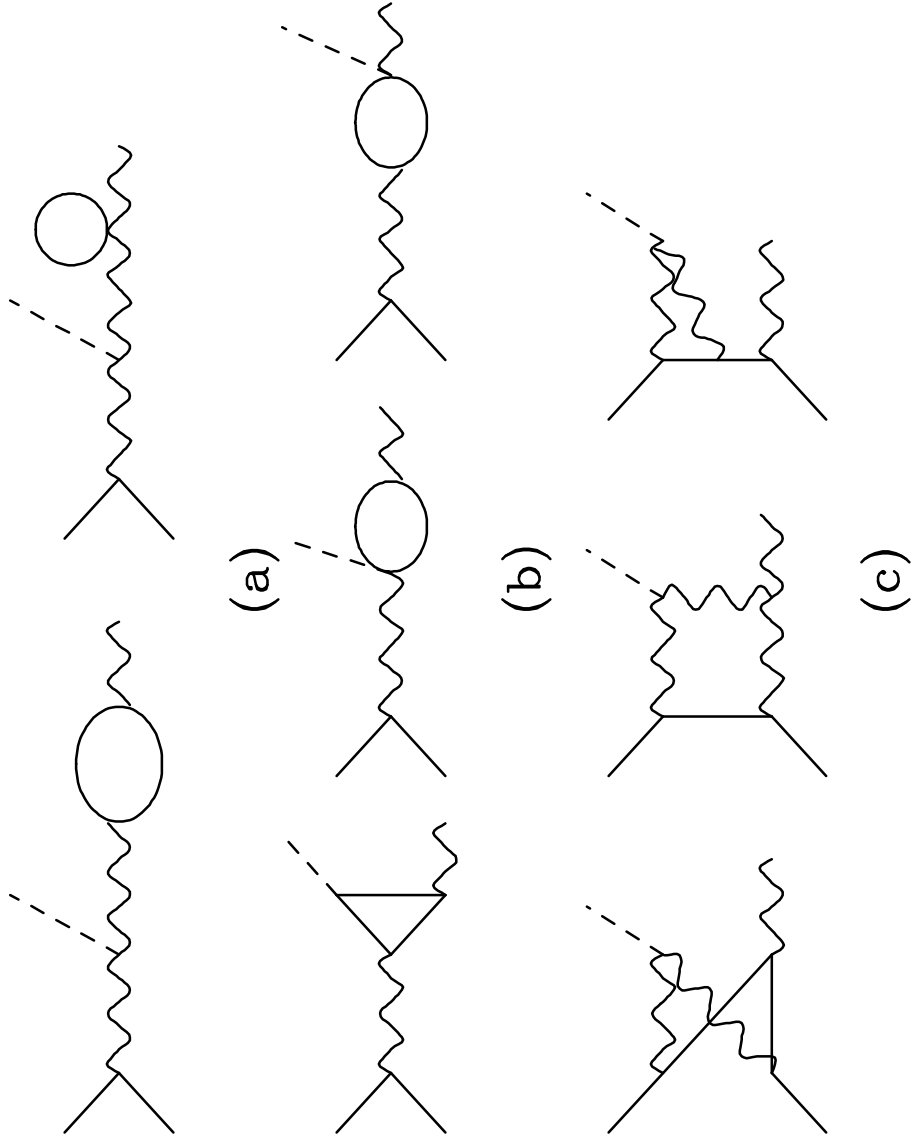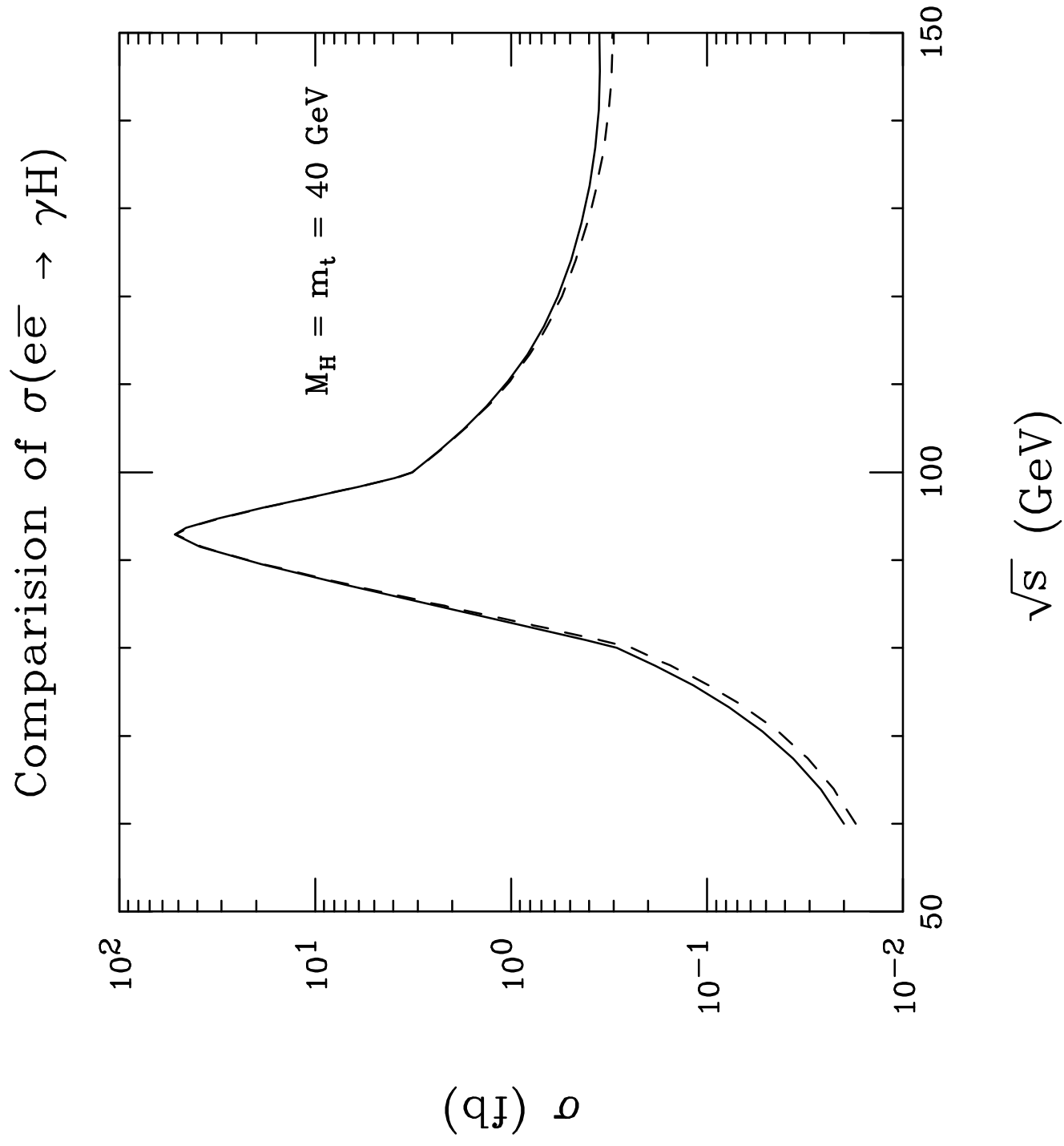
TABLES

TABLE I. Contributions to the Z^0 double pole corrections.

$$\mathcal{M}_{\mu\nu} = (eg^2/m_Z)(\alpha + \beta \tan^2\theta_W)\delta_{\mu\nu}$$

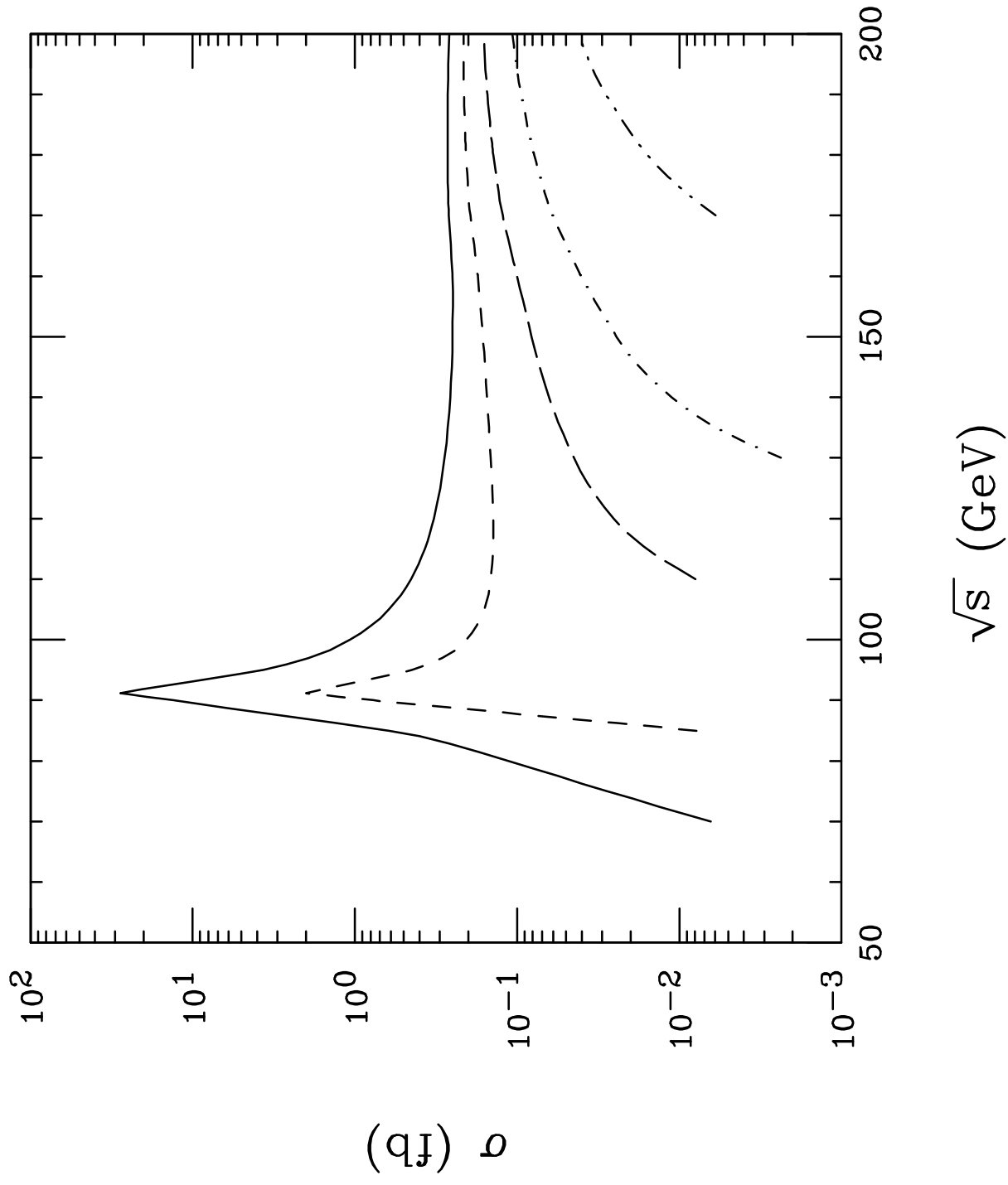| One-Point			Two-Point		
Loop	α	β	Loop	α	β
W	$2nA_0$	0	WW	$-4(A_0 - m_W^2 B_0)$	0
G	A_0	$-A_0$	GG	$-(2/n)(A_0 - m_W^2 B_0)$	$(2/n)(A_0 - m_W^2 B_0)$
θ	$-4A_0$	0	$\theta\theta$	$(8/n)(A_0 - m_W^2 B_0)$	0

TABLE II. A comparison of linear and nonlinear gauge contributions to $\sigma(e\bar{e} \to H\gamma)$ is presented. For any contribution, the result of Ref. [1] is given in the left column and that of the present calculation in the right. The contributions are in femtobarns.

$\sqrt{s}$	$|\mathcal{M}_{\mathrm{Pole}}^Z|^2$		$|\mathcal{M}_{\mathrm{Pole}}^\gamma|^2$		$2\Re e(\mathcal{M}_{\mathrm{Pole}}^{Z\,*}\mathcal{M}_{\mathrm{Pole}}^\gamma)$		$|\mathcal{M}_{\mathrm{Box}}|^2$		$2\Re e(\mathcal{M}_{\mathrm{Pole}}^*\mathcal{M}_{\mathrm{Box}})$	
60	.0069	.0072	.012	.017	−.0014	−.0034	.00027	.00019	−.00029	−.00036
80	.21	.26	.0038	.024	−.0044	−.025	.0022	.0015	.031	.025
m_Z	51	52	.062	.066	.11	.10	.0055	.0039	.097	.026
100	3.3	3.2	.087	.085	.083	.17	.0084	.006	−.29	−.25
120	.61	.57	.15	.14	.047	.088	.025	.018	−.28	−.24
150	.53	.45	.31	.26	.064	.11	.14	.099	−.74	−.57

18

(a)

(b)

(c)

Comparision of $\sigma(e\bar{e} \to \gamma H)$

$M_H = m_t = 40$ GeV

$\sqrt{s}$ (GeV)

σ (fb)

p_1 p_2

2

3

1 q

4

(a)

p_4 p_3

p_1 p_2

2

3

1 q

4

(b)

p_4 p_3